ioMosaic®
Minimizing risk. Maximizing potential.®

Consistency and Limitations of API-521 Equation A.1

Pool Fires

An ioMosaic® Publication

G. A. Melhem, Ph.D., FAIChE

This page is intentionally left empty

IOMOSAIC® CORPORATION

Consistency and Limitations of API-521 Equation A.1
Pool Fires

Process Safety and Risk Management Practices

authored by

G. A. Melhem, Ph.D., FAIChE

Printed April 6, 2026

This page is intentionally left empty

Notice:

This document was prepared by ioMosaic® Corporation (**ioMosaic**) for Public Release. This document represents ioMosaic's best judgment in light of information available and researched prior to the time of publication.

Opinions in this document are based in part upon data and information available in the open literature, data developed or measured by ioMosaic, and/or information obtained from ioMosaic's advisors and affiliates. The reader is advised that ioMosaic has not independently verified all the data or the information contained therein. This document must be read in its entirety. The reader understands that no assurances can be made that all liabilities have been identified. This document does not constitute a legal opinion.

No person has been authorized by ioMosaic to provide any information or make any representation not contained in this document. Any use the reader makes of this document, or any reliance upon or decisions to be made based upon this document are the responsibility of the reader. ioMosaic does not accept any responsibility for damages, if any, suffered by the reader based upon this document.

Revision Log:

Revision 0: October 7, 2025
Revision 1: December 10, 2025

...

Table of Contents

List of Figures

List of Tables

1 Introduction

Upon ignition, a spilled combustible liquid pool will burn in the form of a large turbulent diffusion flame. Calculating the incident flux to an observer or to plant equipment involves four steps: (a) geometric characterization of the flame, (b) estimation of flame thermal radiation properties, (c) estimation of the atmospheric attenuation coefficients, and (d) computation of the geometric view factors between the observer or plant equipment and flame.

The size of the flame will depend upon the spill surface and thermochemical properties of the spilled liquid. In particular, the diameter of the fire (if not confined by a dike), the visible height of the flame, the tilt and drag of the flame caused by wind, and the burning velocity of the liquid.

Figure 1: Pool fire overall energy balance

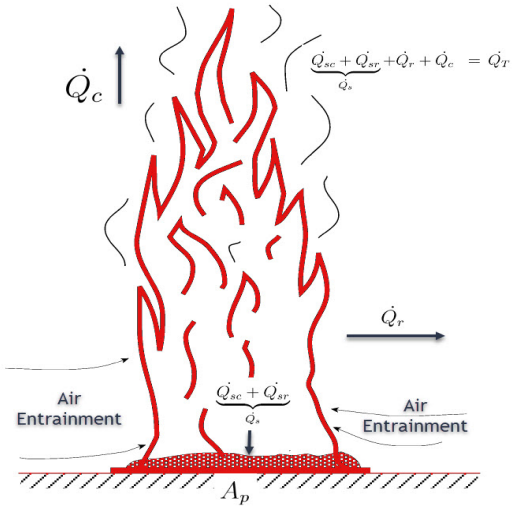

The radiative output of the flame will depend on the fire size, the extent of mixing with air, and the flame surface temperature. Some fraction of the thermal radiation is absorbed by carbon dioxide and water vapor in the intervening atmosphere. In addition, large combustible liquids pool fires produce thick smoke which can significantly obscure flame radiation. Finally, the incident flux at an observer location will depend on the thermal radiation view factor, which is a function of the distance from the flame surface, the observer's orientation, and the flame geometry.

In recent editions of API-521 [4, 6], a fundamental equation (Annex A, A.1) for incident fire flux is provided. Equation A.1 enables a better assessment of both relief requirement and vessel integrity depending on fire type and duration. However, reasonable values of the flame emissivity, ϵ, and the average and peak flame surface temperatures, T_f, are required to calculate thermal radiation heat transfer rates to equipment and vessel surfaces that are either engulfed by the fire or exposed to thermal radiation from the fire. The vessel outer wall temperature, inner wall temperature, and heat transfer rates to the vessel vapor and liquid contents, all depend on the temperature difference between the flame surface and the vessel outer wall surface. Credible vessel wall temperatures are required to assess the estimated time to failure or estimated time to yield. Vessel wall temperatures cannot be calculated properly without reasonable values of the flame average and peak surface temperatures.

The performance of API-521 [4, 6] equation A.1 is evaluated using the proposed default values of emissivity (ϵ) and flame temperature (T_f) for a variety of fuel types. The recommended peak values for LNG are $\epsilon \simeq 1$, $T_f \simeq 1,500$ K and the recommended values for ethanol are $\epsilon \simeq 0.18$, $T_f \simeq 1,273$ K.

2 Overall Energy Balance

The maximum amount of energy release rate by a pool fire can be directly calculated from the liquid burning rate and the heat of combustion of the liquid:

$$\dot{Q}_T \;=\; A_p\,\dot{q}_T = A_p\,\dot{m}\,\Delta H_c = \dot{M}\Delta H_c \tag{1}$$

where A_p is the burning pool surface area in m^2, $\dot{q}_T$ is the total available rate of combustion energy in $\mathrm{W/m^2}$, $\dot{Q}_T$ is the total available rate of combustion energy in W, $\dot{m}$ is the mass burning rate in $\mathrm{kg/m^2/s}$, $\dot{M}$ is the total mass burning rate in $\mathrm{kg/s}$, and ΔH_c is the heat of combustion in $\mathrm{J/kg}$. However, the pool combustion reaction is not 100 % efficient and combustion energy is lost or scattered by convection to the surroundings. Furthermore, energy is radiated and conducted by the flame to the liquid pool surface and energy is also radiated by the flame surface to the surroundings and plant equipment (see Figure 1).

It is reasonable to assume, for hazard and safe exclusion zones estimates, that 100 % of the combustion energy goes into heating the pool reactants, entrained air, and combustion products to the flame temperature at the upper flammability limit, T_f. Radiation from the flame surface heats the pool liquid materials to the boiling point. The pool surface then becomes fuel rich and the furthest distance from the pool liquid surface where combustion becomes possible is the point at the which the pool vapors are diluted by ambient air to the upper flammability limit.

$$\underbrace{\dot{Q}_{sc} + \dot{Q}_{sr}}_{\dot{Q}_s} + \dot{Q}_r + \dot{Q}_c \;=\; \chi_a \dot{M}\Delta H_c = \chi_a \dot{Q}_T \tag{2}$$

where $\dot{Q}_s$ is the overall rate of combustion energy transported from the fire to the pool liquid surface, $\dot{Q}_{sr}$ is the rate of combustion energy radiated by the flame and is visible to the pool surface, $\dot{Q}_{sc}$ is the rate of combustion energy convected and/or conducted to the pool surface, $\dot{Q}_r$ is the rate of combustion energy radiated by the fire in all directions to the surroundings (except to the liquid pool surface), $\dot{Q}_c$ is the rate of combustion energy scattered or lost to the atmosphere by convection from the buoyant fire plume, and χ_a is the total combustion process efficiency. The vast majority of the energy gained by the liquid pool surface is attributed to radiation, ($\dot{Q}_{sr} \simeq 0.65 \times \dot{Q}_s$).

Figure 2: Measurements of χ_s, χ_r, and χ_c as a function of the mass burning flux of methane and natural gas in a 0.38 m burner [1]

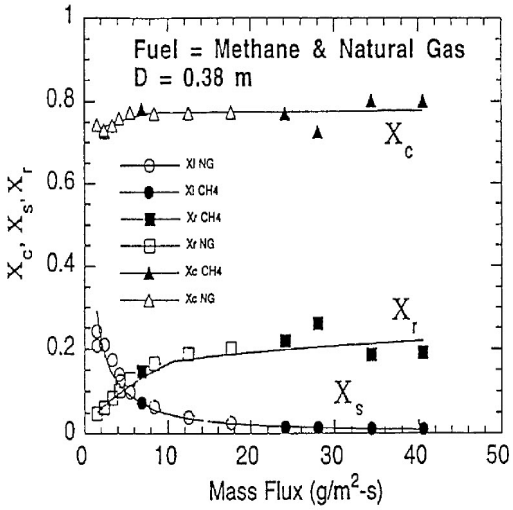

In general [1], up to $\simeq$ 25 % of the flame radiation energy is fed back and gained by the pool surface ($\dot{Q}_s$), up to $\simeq$ 25 % is radiated to the surroundings and plant equipment ($\dot{Q}_r$), and up to $\simeq$ 50 % is lost or scattered by convection to the atmosphere ($\dot{Q}_c$). This is illustrated in Figure 2.

The fraction of total combustion energy attributed to thermal radiation is obtained by dividing equation 2 by $\dot{Q}_T$:

$$\underbrace{\chi_{sc} + \chi_{sr}}_{\chi_s} + \chi_r + \chi_c = \chi_a \simeq 1 \tag{3}$$

where χ_s is the overall fraction of combustion energy transported from the fire to the pool liquid surface, χ_{sr} is the fraction of total combustion energy radiated by the flame and is visible to the pool surface [1], χ_{sc} is the fraction of total combustion energy convected and/or conducted to the pool surface, χ_r is the fraction of total combustion energy radiated by the fire in all directions to the surroundings (except to the liquid pool surface), χ_c is the fraction of total combustion energy scattered or lost to the atmosphere by convection from the buoyant fire plume, and χ_a is the total combustion process efficiency.

The maximum possible fraction of total combustion energy available for thermal radiation, χ_{r_T}, becomes:

$$\chi_{r_T} = \chi_r + \chi_{sr} \quad = \quad \frac{A_f \epsilon \sigma T_f^4}{\dot{M} \Delta H_c} + \frac{\dot{Q}_{sr}}{\dot{M} \Delta H_c} = \frac{A_f \epsilon \sigma T_f^4}{\dot{Q}_T} + \frac{\dot{Q}_{sr}}{\dot{Q}_T} \tag{4}$$

where ϵ is the flame emissivity, $\sigma = 5.67 \times 10^{-8}$ W/(m^{2}K^4) is the Stefan-Boltzmann constant, A_f is the total surface area of the flame in m^2, and $A_f \epsilon \sigma T_f^4$ is the total available flame radiation energy to the surroundings and plant equipment.

The average pool flame temperature has to be computed using a chemical equilibrium computer code such as SuperChems® Expert with a starting vapor temperature equal to the normal boiling point of the pool burning mixture or chemical. For pool fires where sufficient confinement is provided, most of the combustion energy, $\dot{Q}_r + \dot{Q}_c$, will be absorbed by nearby confined equipment and surfaces.

3 API-521 Fire Flux and Flame Emissive Power

In recent editions of API-521 [4, 6], a fundamental equation (Annex A, A.1) for incident fire flux is provided. Equation A.1 enables a better assessment of both relief requirement and vessel integrity depending on fire type and duration.

$$I_{fire,w} \quad = \quad \underbrace{\alpha_w \epsilon_f \sigma T_f^4}_{\text{Radiative Flux}} + \underbrace{h\left(T_{f,g} - T_{w,t}\right)}_{\text{Convective Flux}} - \underbrace{\epsilon_w \sigma T_{w,t}^4}_{\text{Re-radiated Flux}} \tag{5}$$

The first term in Equation 5 is the flame radiative heat flux into the external wall or insulation surface. The second term is the hot combustion gases convective heat flux into the external wall or insulation surface. The third term is the heat flux that is re-radiated by the external wall or insulation surface. Note that temperature in this equation must be absolute. The radiative heat flux is the dominant component of fire flux.

A vessel or piping segment does not have to be engulfed by fire in order to receive large heating rates by thermal radiation [7]. Thermal radiation is independent of elevation, which is why fire

[1] χ_{sr} includes a geometric view factor correction.

heating of vessels and equipment should not be limited to vessel sections or vessels that are only within the 25 feet elevation [8] limit used by API-521 or the 30 ft limit used by NFPA-30. This is especially important for vessels containing reactive chemicals.

When SI units are used, $I_{fire,w}$ is the net heat flux reaching the outer wall or insulation surface in $\mathrm{W/m^2}$, α_w is the external wall surface or insulation absorptivity, ϵ_f is the flame surface emissivity, σ is the Stefan-Boltzmann constant = $5.67 \times 10^{-8}\ \mathrm{W/m^2/K^4}$, T_f is the flame surface temperature in K, h is the combustion gases convective heat transfer coefficient in $\mathrm{W/m^2/K}$, $T_{f,g}$ is the combustion gases temperature in K, $T_{w,t}$ is the time dependent wall surface temperature, and ϵ_w is the outer wall or insulation surface emissivity (note that hydrocarbons fire exposure scenarios can cause the vessels walls to be coated with soot).

Table 1: Recommended parameter values for Equation 5 for flame jets by API-521 [4] where other data or information are not available

		Flame Jet			
Parameter	Description	Surface Average Heat Flux		Local Peak Heat Flux	
Leak rates		>2 kg/s (Large Jet)	≤2 kg/s (Small Jet)	>2 kg/s (Large Jet)	≤2 kg/s (Small Jet)
ε_f	Flame emissivity	0.33	NA	0.87	0.75
ε_w	Wall emissivity	0.75	NA	0.75	0.75
α_w	Wall absorptivity	0.75	NA	0.75	0.75
h	Convective heat transfer coefficient between equipment and surrounding air	40 W/m^2 K	NA	100 W/m^2 K	90 W/m^2 K
T_g	Temperature of combustion gases flowing over the surface	1,173 K (900°C)	NA	1,473 K (1,200°C)	1,373 K (1,100°C)
T_f	Fire temperature	1,373 K (1,100°C)	NA	1,473 K (1,200°C)	1,373 K (1,100°C)
q_f	Fire heat flux	100 kW/m^2	NA	350 kW/m^2	250 kW/m^2
q_w	Absorbed heat flux	85 kW/m2	NA	290 kW/m^2	210 kW/m^2

Table 2: Recommended parameter values for Equation 5 for pool fires by API-521 [4] where other data or information are not available

		Pool Fire	
Parameter	Description	Surface Average Heat Flux	Local Peak Heat Flux
ε_f	Flame emissivity	0.75	0.75
ε_w	Equipment emissivity	0.75	0.75
α_w	Equipment absorptivity	0.75	0.75
h	Convective heat transfer coefficient between equipment and surrounding air	20 W/m^2 K	20 W/m^2 K
T_g	Temperature of combustion gases flowing over the surface	873 K (600°C)	1,323 K (1,050°C)
T_f	Fire temperature	1,023 K (750°C)	1,323 K (1,050°C)
q_f	Fire heat flux	60 kW/m^2	150 kW/m^2
q_w	Absorbed heat flux	45 kW/m2	120 kW/m^2

Recommended values are provided by API-521 [4] for a typical unconfined heptane pool fire en-

gulfing an uninsulated carbon steel vessel for a surface average heat flux ($\alpha_w = 0.75$, $\epsilon_f = 0.75$, $T_f = 750\ ^\circ\mathrm{C}$ (1023 K), $h = 20\ \mathrm{W/m^2/K}$, $T_{f,g} = 600\ ^\circ\mathrm{C}$ (873 K), and $\epsilon_w = 0.75$) and local peak heat flux parameters ($\alpha_w = 0.75$, $\epsilon_f = 0.75$, $T_f = 1050\ ^\circ\mathrm{C}$ (1323 K), $h = 20\ \mathrm{W/m^2/K}$, $T_{f,g} = 1050\ ^\circ\mathrm{C}$ (1323 K), and $\epsilon_w = 0.75$). These recommended values are consistent with a fire flux of 60 $\mathrm{kW/m^2}$ and 150 $\mathrm{kW/m^2}$ for surface-averaged and local peak values and wall absorbed values of 45 $\mathrm{kW/m^2}$ and 120 $\mathrm{kW/m^2}$, respectively. Recommended values for jet fires are also provided by API-521 [4] (as shown in Table 1) where actual test data are not readily available for establishing the flame characteristics.

API-521 [4] also provides an empirical equation to directly calculate the heating rate absorbed by the vessel contents since Equation A.1 (5) only provides the fire flux that the vessel outer wall or insulation is exposed to. The heating rate absorbed by vessel contents is calculated empirically [4]:

$$Q_{fire} = qFA_w^a \tag{6}$$

Where Q_{fire} is the total heating rate absorbed by the liquid in $\mathrm{J/s}$ or Watts (W), F is a mitigation factor that is used to allow reduction of the heating rate because of water sprays, firefighting, and/or insulation, and A_w is the wetted surface area in $\mathrm{m^2}$, i.e. the inner wall surface area contacted by liquid. The constant q represents the heat flux absorbed by the liquid corrected for the presence of adequate drainage. Note that q includes a unit conversion factor associated with the fact that the wetted surface area is raised to a power less than 1. A similar form is used by NFPA-30 [9]. Also note that NFPA and API correlations differ for wetted surface areas that are less than 2,800 $\mathrm{ft^2}$ where NFPA yields a higher heating rate.

Equation 6 correlates the heat absorbed by the vessel liquid contents to the wetted surface area raised to the power $a = 0.82$ typically. Confined pool fires lead to higher heating rates because higher fractions of the fire radiative and convective are recovered due to confinement and secondary combustion. A value of $a = 1$ is substituted for $a = 0.82$ in API-521.

Melhem [10] showed that the simple API-521 equation (Equation 6) can be recovered from Equation 5 when the fire heating and relief dynamics are properly modeled. Equation 5 can be used to develop both the relief requirements and to assess the failure potential as well as the effectiveness of a variety of potential mitigation options. Melhem [10] also independently demonstrated that Equation 5, when used with Process Safety Office® SuperChems® Expert vessel and wall dynamics, can accurately reproduce measured large scale [11, 12, 13] fire exposure test data including wall temperatures and vessel failure pressure.

The fire flux provided by Equation 5 is used by detailed dynamic simulation software such as SuperChems® Expert to provide time dependent estimates of wall segment temperatures, estimated time to failure, fluid temperatures, and single/multiphase venting rates with and without chemical reactions. Because it is difficult to establish consistent values of ϵ_f and T_f, and because ϵ_f and T_f are flame surface location dependent, it is recommended that average values should be used to size the relief requirements or relief device, and peak values should be used to establish time to failure and wall temperatures.

4 Consistency of API-521 Equation A.1

API-521 [4, 6] allows the use of the Annex A (Equation A.1) for pressure relief sizing, but cautions the user to justify the heat transfer parameters used for the analysis. API-521 recognizes the limitations of Equation A.1 and warns the user:

Section A.3.1 "The analytical method can be used as an alternative to the empirical method for calculation of the size of PRDs and the pressure profile, both of which involve the surface average heat flux."

Section A.3.1 "the analytical method is based on heat transfer calculations that require specification of a number of variables that characterize details of the fire and heat transfer characteristics (e.g. fire temperature, emissivities, heat transfer coefficient, etc.). Because the range in these variables can vary significantly, a wide range in fire heat inputs can be obtained. Hence, it is important to understand the basis of the variables and ensure the selected values for the variables are representative of the fire scenario being evaluated (e.g. be careful when using data from different fire tests)."

Section A.3.2 "However, when calculating the surface average heat input to the equipment for use in sizing PRDs, for example, a temperature less than the fire temperature, T_{fire}, is recommended because the average temperature of the combustion gases flowing over the fire-exposed surface will be less than the fire temperature."

For pool fires, API-521 [4, 6] recommends an average flame temperature of 1,023 K and a peak flame temperature of 1,323 K along with a flame emissivity of 0.75, where measured and/or other data is not available. We can prove that these values have to be consistent and are strongly dependent on fuel type.

For a circular pool fire with a diameter of D_p and a visible flame length of L_f, we can calculate the flame surface area assuming a flame cylindrical geometry:

$$A_f = \pi D_p L_f \tag{7}$$

If a measured value of χ_r is provided, we can use Equation 4 to calculate either the average flame surface temperature, or the flame surface emissivity, or the burning rate:

$$\chi_r = \frac{A_f \epsilon \sigma T_f^4}{\dot{Q}_T} = \left(\frac{A_f}{A_p}\right)\left(\frac{\epsilon \sigma T_f^4}{\dot{m}\Delta H_c}\right) \tag{8}$$

For a cylindrical flame shape and a large pool diameter, it can be shown (see Equation 30, $\frac{L_f}{D_p} \simeq 1.73$) that $A_f/A_p \simeq 7.5$, or:

$$\chi_r = \left(\frac{7.5}{\dot{m}\Delta H_c}\right)\epsilon \sigma T_f^4 \tag{9}$$

We can approximate $\dot{m}$ using Equation 21:

$$\dot{m} = 0.001\frac{\Delta H_c}{\Delta H_v} \tag{10}$$

This will yield the following expression for χ_r:

$$\chi_r = \left(\frac{7,500\ \Delta H_v}{\Delta H_c^2}\right)\epsilon\sigma T_f^4 \tag{11}$$

Equation 11 shows that the fraction radiated, χ_r, is a strong function of flame temperature, flame emissivity, and the fuel burning rate.

Radiometer measurements from large scale fire experiments suggest that χ_r decreases with increasing pool fire diameter:

$$\chi_r = \chi_{r_{\max}} e^{-kD_p} \tag{12}$$

where $\chi_{r_{\max}} = 0.35$ and $k = 0.05\ \mathrm{m}^{-1}$ based on limited large scale hydrocarbon pool fires data [14]. Both Equations 11 and 12 are consistent. Larger pool diameters lead to less air entrainment by the pool fire, incomplete combustion, and as a result lower emissivity and flame temperatures.

Equation 8 requires that the values selected for flame temperature, burning rate, heat of combustion, and flame emissivity are consistent such that they do not yield unreasonable values of χ_r. As a result, the default API-521 recommended values are not suitable for all fuels as shown in Tables 3 and 4. The recommended default values of ϵ and T_f are most suitable for hydrocarbon fuels only. Fuels other than hydrocarbons require specific values of ϵ and T_f based on actual measurements.

As shown by Table 3 the hydrocarbon predictions of χ_r at the recommended default values of ϵ and T_f are reasonable for both average and peak values for large diameter pool fires (see Figure 6) while the predictions for hydrogen are not. Although the emissivity of hydrogen, $\epsilon \simeq 0.1$, is less than 0.75 due to the absence of soot, the fraction of hydrogen combustion energy should be higher because of a higher flame temperature. Typical measured hydrogen flames radiative fractions range from 6 % to 12 % [15, 16].

Low carbon alcohol flames are also less emissive than hydrocarbon flames, $\epsilon \simeq 0.1$, primarily because they undergo more complete combustion, resulting in significantly less production of glowing solid soot particles. Alcohol molecules (e.g., methanol, ethanol) contain oxygen atoms within their molecular structure (the hydroxyl group, OH). This internal oxygen allows alcohols to mix and burn more completely with air, requiring less additional oxygen to achieve full oxidation.

The bright, yellow-orange luminosity characteristic of hydrocarbon flames comes from the incandescence of hot soot that forms during incomplete combustion. Because alcohols burn more cleanly and efficiently, less soot particles are created. Alcohols typically used as fuels, such as methanol and/or ethanol, have shorter carbon chains compared to many components in gasoline or other liquid hydrocarbons. Shorter chains and lower carbon density in the molecule make it harder to form the large aggregates of carbon atoms required for soot formation. Because of low flame emissivity, more flame combustion energy is lost by convection than radiated from the flame surface. As shown in Table 4, the predicted radiation fraction of combustion energy is significantly overestimated for some alcohols and CHO compounds.

Measured peak χ_r values for methanol, ethanol, and acetone (see [17]) are reported to be 24 %, 26 %, and 31 % respectively. In 1989, the Association of Canadian Distillers conducted large scale testing with ethanol [18] where they measured flame temperatures ranging from 600 °C (873 K) to 1,000 °C (1,273 K) and average fire flux values ranging from 25 to 50 $\mathrm{kW/m^2}$.

The default values of API-521 Equation A.1 should only be used for hydrocarbon fuels where the calculated maximum fraction of combustion energy radiated (see Equation 11) does not exceed $\simeq 35\ \%$.

Figure 3: Large scale ethanol fires test vessel and arrangement

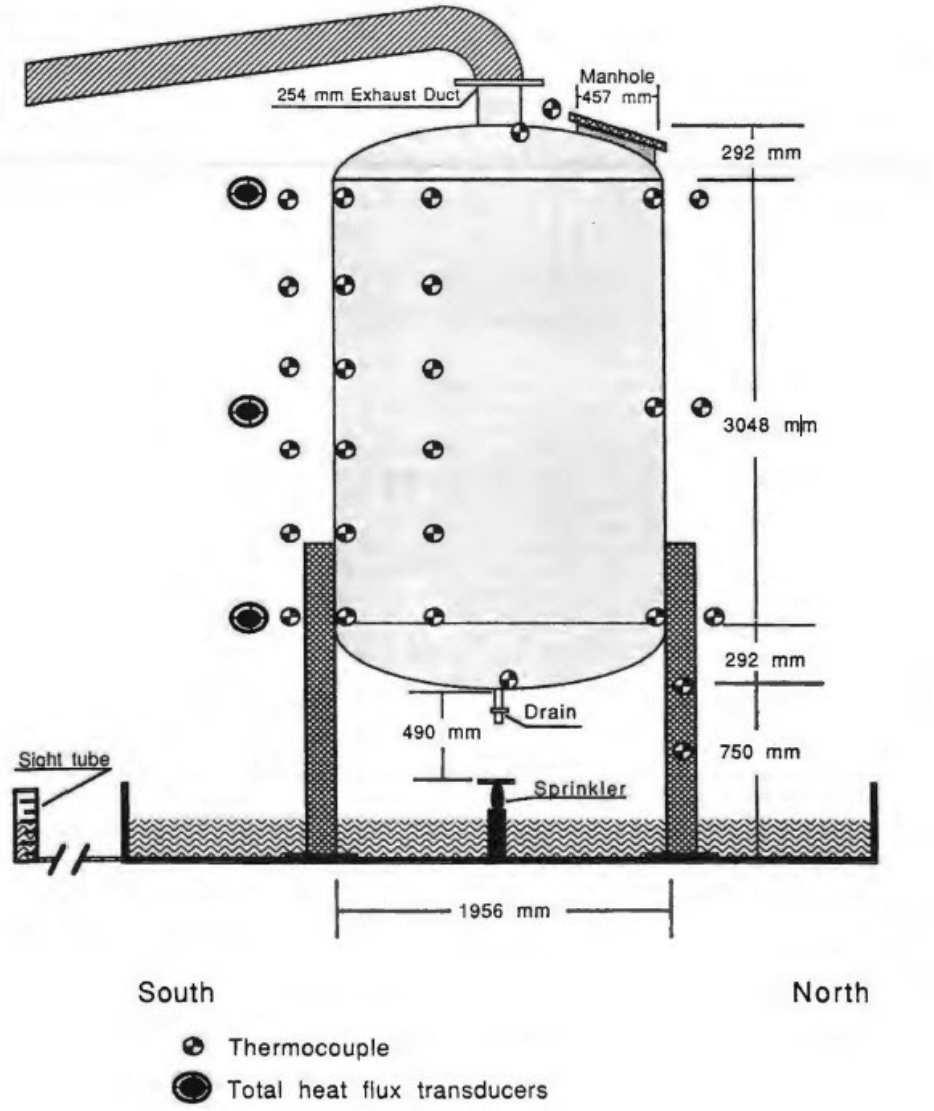

Source: [18]

Table 3: Calculated fraction radiated, χ_r, using API-521 recommended values of $\epsilon = 0.75$, $T_f = 1,023$ K (average fire flux), and $T_f = 1,323$ K (peak fire flux) for hydrogen and selected hydrocarbons

Fuel	Chemical Formula	$\dot{m}$ kg/(m^{2}s)	T_b K	ΔH_v kJ/kg	ΔH_c MJ/kg	$\frac{\Delta H_c}{\Delta H_v}$	LFL_{T_b} vol %	UFL_{T_b} vol %	χ_r %, @1,023K	χ_r %, @1,323K
Hydrogen	H_2	0.271	20.39	442.76	119.96	270.93	7.60	71.40	1.07	3.01
Methane	CH_4	0.098	111.66	510.12	50.01	98.04	5.73	14.27	7.12	19.93
Ethane	C_2H_6	0.097	184.55	488.51	47.51	97.26	3.25	12.25	7.56	21.15
Propane	C_3H_8	0.109	231.11	426.32	46.33	108.68	2.20	9.40	6.94	19.40
n-Butane	C_4H_{10}	0.118	272.65	385.99	45.72	118.45	1.83	8.47	6.45	18.04
n-Pentane	C_5H_{12}	0.125	309.22	369.92	44.98	121.58	1.39	7.81	6.39	17.87
n-Hexane	C_6H_{14}	0.132	341.88	371.05	44.74	120.57	1.16	7.54	6.48	18.12
Benzene	C_6H_6	0.102	353.24	432.57	40.14	92.80	1.35	7.16	9.38	26.23
n-Heptane	C_7H_{16}	0.141	371.58	364.07	44.56	122.39	0.95	7.05	6.41	17.92
n-Octane	C_8H_{18}	0.146	398.83	359.41	44.42	123.59	0.74	6.56	6.36	17.80
n-Nonane	C_9H_{20}	0.153	423.97	356.41	44.33	124.37	0.63	5.67	6.34	17.72
n-Decane	$C_{10}H_{22}$	0.157	447.31	348.87	44.24	126.80	0.73	5.47	6.23	17.42
n-Dodecane	$C_{12}H_{26}$	0.169	489.47	354.35	44.11	124.48	0.52	4.78	6.36	17.80
Triacontane	$C_{30}H_{62}$	0.264	722.85	332.56	43.59	131.07	0.23	3.17	6.11	17.10

Source: SuperChems® Expert

Table 4: Calculated fraction radiated, χ_r, using API-521 recommended values of $\epsilon = 0.75$, $T_f = 1,023$ K (average fire flux), and $T_f = 1,323$ K (peak fire flux) for alcohols and selected CHO compounds

Fuel	Chemical Formula	$\dot{m}$ $\mathrm{kg/(m^2 s)}$	T_b K	ΔH_v kJ/kg	ΔH_c MJ/kg	$\frac{\Delta H_c}{\Delta H_v}$	LFL_{T_b} vol %	UFL_{T_b} vol %	χ_r %, @1,023K	χ_r %, @1,323K
Methanol	CH_4O	0.018	337.85	1184.55	19.91	16.81	7.11	36.20	104.33	291.85
Ethanol	C_2H_6O	0.031	351.44	940.49	26.82	28.52	4.17	19.14	45.68	127.77
Acetone	C_3H_6O	0.056	329.44	540.38	28.57	52.87	2.54	12.86	23.13	64.70
n-Propanol	C_3H_8O	0.045	370.35	793.27	30.68	38.68	1.88	12.12	29.44	82.34
Isopropanol	C_3H_8O	0.046	355.41	751.37	30.45	40.53	1.90	12.10	28.31	79.18
Glycerol	$C_3H_8O_3$	0.02	563.15	993.37	16.04	16.14	2.14	19.56	134.91	377.39
Methyl ethyl ketone	C_4H_8O	0.072	352.79	476.33	31.36	65.85	1.72	10.08	16.91	47.31
Diethyl ether	$C_4H_{10}O$	0.092	307.58	374.11	33.78	90.28	1.89	48.01	11.46	32.04
n-Butanol	$C_4H_{10}O$	0.057	390.81	706.24	33.13	46.92	1.28	11.32	22.47	62.85
Isobutanol	$C_4H_{10}O$	0.056	380.81	741.41	33.04	44.56	1.59	11.01	23.72	66.36
1-Pentanol	$C_5H_{12}O$	0.068	410.95	655.66	34.72	52.95	1.08	10.12	19.00	53.15
n-Butyl acetate	$C_6H_{12}O_2$	0.09	399.15	374.21	28.26	75.53	1.60	7.70	16.36	45.78
1-Hexanol	$C_6H_{14}O$	0.08	430.15	590.11	35.96	60.94	1.09	8.31	15.94	44.59
1-Heptanol	$C_7H_{16}O$	0.088	449.45	586.27	36.91	62.95	0.89	7.31	15.03	42.06
1-Octanol	$C_8H_{18}O$	0.099	468.35	541.28	37.62	69.50	0.79	6.51	13.36	37.37
1-Nonanol	$C_9H_{20}O$	0.107	486.25	530.90	38.13	71.82	0.69	6.21	12.75	35.68
1-Decanol	$C_{10}H_{22}O$	0.117	503.35	500.88	38.65	77.16	0.60	5.61	11.71	32.77
1-Dodecanol	$C_{12}H_{26}O$	0.135	535.00	470.54	39.38	83.69	0.50	5.20	10.60	29.65
Oleic Acid	$C_{18}H_{34}O_2$	0.151	633.00	391.03	37.17	95.06	0.30		9.88	27.65
Methyl Oleate	$C_{19}H_{36}O_2$	0.174	617.00	338.44	37.44	110.62	0.31	7.89	8.43	23.59
Monoolein	$C_{21}H_{40}O_4$	0.175	714.00	333.65	33.45	100.24	0.29	3.21	10.42	29.14

Source: SuperChems® Expert

Figure 4: Measured ethanol fire test data for Test 1

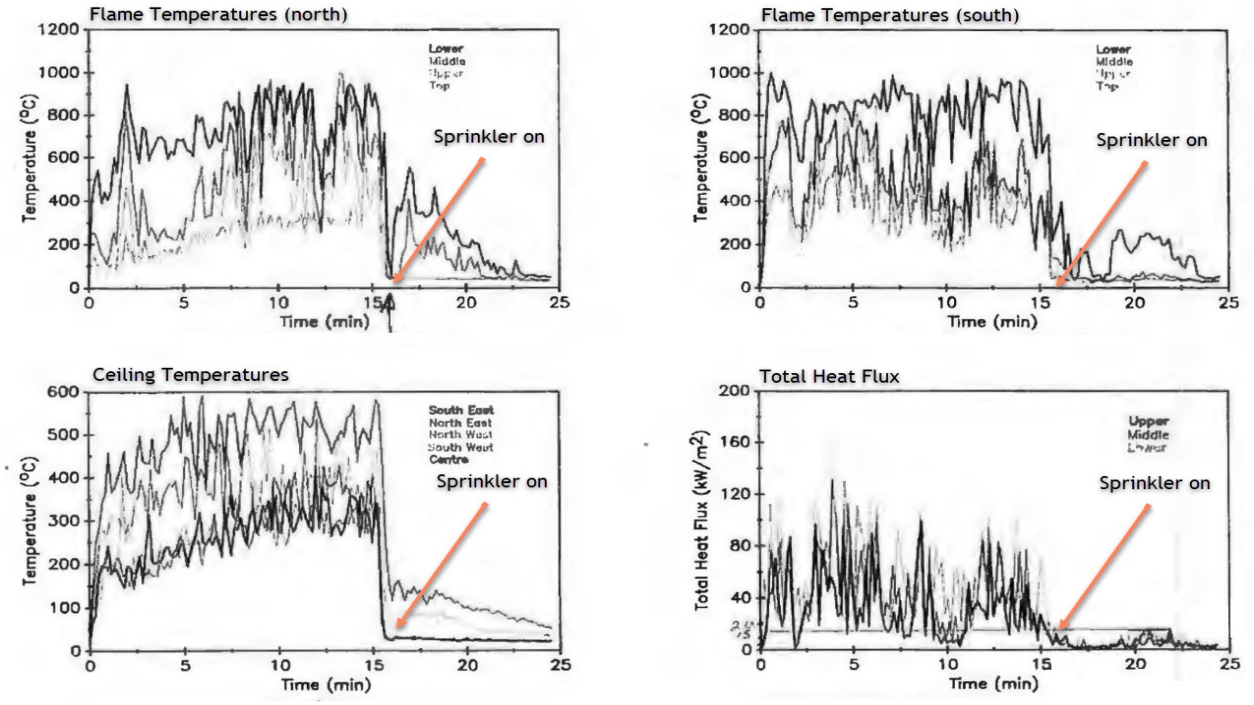

Source: [18]

5 Biofuels Pool Fires

In 1989, the National Research Council of Canada published a report summarizing large scale test data for ethanol and hexane pool fires [18]. The fire tests were commissioned by the Association of Canadian Distillers and were conducted to evaluate the behavior of stainless steel tanks storing high-proof ethanol under fire conditions and to evaluate the effectiveness of water spray protection for tanks containing distilled spirits.

A 2,600 gal vertical cylindrical vessel (see Figure 3), 16 gauge, stainless steel vessel was exposed to ethanol and hexane fires. The test vessel was equipped with several sensors to measure heat flux, internal fluid temperatures, and external wall temperatures. The vessel had an open 10 inch vent to atmosphere to keep the internal pressure at ambient pressure. In test 1, the vessel was filled to capacity with water. A free burn was conducted (see Figure 4).

As shown by Figure 4, measured flame temperatures ranged from 600 °C (873 K) to 1,000 °C (1,273 K) and average fire flux values ranged from 25 to 50 $\mathrm{kW/m^2}$. The measured average ethanol fire heat flux was approximately 30.6 $\mathrm{kW/m^2}$ and the heat absorbed by the water inside the vessel was estimated at 56 % [2] of what would be predicted by Equation 6 where the total vessel wetted area is 266 $\mathrm{ft^2}$. The heating rate for water was estimated at 1.11 °C/min from the measured water temperature. The vessel wall temperature in the vapor space (unwetted) reached 300 °C .

[2]The measured heating rate for n-hexane was 310 % of what would be predicted by Equation 6.

If we use the reported value of χ_r for ethanol of 26 % [17], and the measured peak flame temperature of 1273 K [18], we can calculate the following flame emissivity, ϵ, using Equation 11:

$$\begin{aligned} \epsilon &= \chi_r \frac{\Delta H_c^2}{7,500\ \Delta H_v} \frac{1}{\sigma T_f^4} \\ &= 0.26 \frac{28.52 \times 26.82 \times 10^6}{7,500} \frac{1}{5.67 \times 10^{-8} 1,273^4} = 0.178 \end{aligned} \tag{13}$$

Using $\epsilon = 0.178$, we calculate an emissive power of:

$$E = \epsilon \sigma T_f^4 = 0.178 \times 5.67 \times 10^{-8} \times 1,273^4 = 26.5 \mathrm{kW/m^2} \tag{14}$$

which is very close to the reported average value of 30.6 $\mathrm{kW/m^2}$. An emissivity of 0.178 is the consistent value to use with a flame temperature of 1,273 K for ethanol.

6 LNG Pool Fires

Figure 5: The LNG value chain

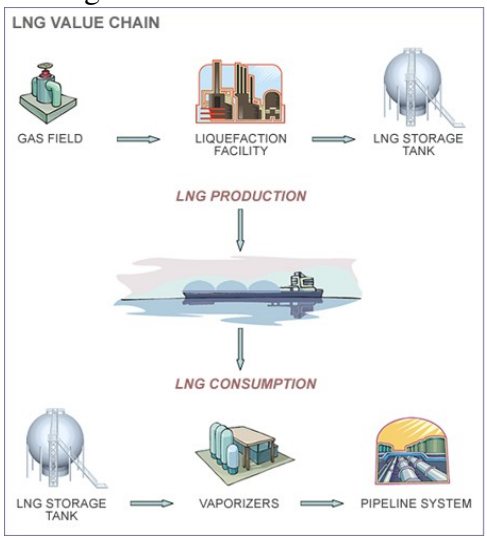

Source:ioMosaic®

Potential LNG pool fires from large LNG tanker spills received a lot of attention to warrant a United States Government Accountability Office (GAO) study and report to the United States Congress in 2007. Because of the large amount of LNG carried by a tanker, currently a Q-Max class tanker has a capacity of 266,000 $\mathrm{m^3}$. There are also large LNG storage tanks on land in LNG terminals and LNG liquefaction facilities. The largest single LNG storage tank in the world is 270,000 $\mathrm{m^3}$, located at Sinopec's Qingdao LNG Terminal in China, with a diameter of 100.6 m and height of 55 m, brought online in late 2023. In addition to LNG transported by tankers and stored in LNG terminals and liquefaction facilities, smaller LNG storage and vaporization facilities exist in the LNG value chain (see Figure 5) with potential for LNG loss of containment hazards and risks, including pool fires on land and water.

The largest known LNG pool fire tests were conducted by Shell [19] and Sandia National Laboratories [20, 21]. Based on the Montoir 35 m pool fires tests [19], the flame surface emissive power of LNG [22] was recommended to be 220 +/- 50 $\mathrm{kW/m^2}$. In 2009, Sandia National Laboratories conducted the larger Phoenix 83 m LNG pool fire tests on water [20] and showed that the LNG flame emissive power can be as high as 326 $\mathrm{kW/m^2}$. Sandia recommended [21] an LNG flame emissive power in the range of 248 to 326 $\mathrm{kW/m^2}$ and a nominal average burning rate of 3.5×10^{-4} $\mathrm{m/s}$ (0.15 $\mathrm{kg/m^2/s}$) and a range of 2.6×10^{-4} (0.11 $\mathrm{kg/m^2/s}$) to 4.5×10^{-4} $\mathrm{m/s}$ (0.19 $\mathrm{kg/m^2/s}$).

The burning rate of LNG is typically equal to twice the boiling rate. For liquid LNG spills on land, the boiling rate ranges from 0.05 to 0.1 $\mathrm{kg/m^2/s}$. For liquid LNG spills on water, the boiling

Table 5: Typical LNG mixture components properties

	Methane	Ethane	Propane	n-Butane	Nitrogen	Carbon Dioxide
Normal Boiling Point. K	111.660	184.550	231.110	272.650	77.352	194.600
Critical Temperature. K	190.580	305.420	369.820	425.180	126.100	304.190
Critical Pressure. bar	46.043	48.801	42.492	37.969	33.944	73.815
Liquid Density at NBP. kg/m3	424.056	544.709	582.964	601.983	807.829	1180.590
Latent Heat of Vaporization. kJ/kg	508.879	488.503	426.317	385.989	197.873	369.586
Lower Flammability Limit. Vol %	5.000	3.000	2.100	1.800		
Upper Flammability Limit. Vol %	15.000	12.500	9.500	8.500		
Auto-ignition Temperature. K	873.000	788.150	723.150	678.150		
Minimum Ignition Energy. mJ	0.29	0.24	0.25	0.25		
Heat of Combustion. MJ/kg	-50.01	-47.51	-46.33	-45.72		
Laminar Burning Velocity. m/s	0.45	0.53	0.52	0.50		
Adiabatic Flame Temperature. K	2,230	2,272	2,283	2,286		
Stoichiometric Concentration. %	9.48	5.66	4.03	3.13		
Detonation cell width. mm	300	55	55	60		
Minimum Critical Energy. kJ	19,200	144	240	240		

Source:ioMosaic®

rate ranges from 0.1 to 0.2 $\mathrm{kg/m^2/s}$. LNG burning rates on land can be as high as 0.14 $\mathrm{kg/m^2/s}$ and as high as 0.3 $\mathrm{kg/m^2/s}$ for LNG pool fires on water. Note that pool/spill surface interface factor [23] can be as large as 6 or 7 for LNG spills on water. Spill surface imperfections such as porosity and surface roughness and interface distortions/turbulence caused by boiling on water surfaces, wave action, and water flow velocity, can increase the conduction heat transfer from the underlying surface to the LNG pool to yield more LNG vaporization.

The flame surface emissive power is also influenced by the size and chemical composition of the burning pool. LNG is not just methane. LNG is a mixture (see Table 5) of hydrocarbons where the methane content in some LNG mixtures can be as low as 85 %.

Figure 6 demonstrates that, unlike other hydrocarbons, the fraction of combustion energy radiated by large LNG pool fires starts to decline at pool diameters larger than 100 m. Equation 12 parameters should be adjusted for LNG fires. Also note that Equation 8 requires that the values selected for flame temperature, burning rate, heat of combustion, and flame emissivity are consistent such that they do not yield unreasonable values of χ_r.

For an LNG pool fire diameter of 83 m (see Figure 6), the measured surface emissive power is 286 $\mathrm{kW/m^2}$. Using the recommended value of $T_f = 1,323$ K, we obtain an emissivity value of:

$$286,000 \quad = \quad \epsilon\sigma T_f^4 \text{ or } \epsilon = \frac{286,000}{5.67 \times 10^{-8} \times 1,323^4} = 1.646 \tag{15}$$

The value of ϵ cannot be larger than that of a blackbody ($\epsilon \leq 1$). As a result the peak temperature value of 1,323 K is not suitable for an 83 meter LNG pool fire. The same expression can be

Figure 6: LNG test data summary for flame surface emissive power

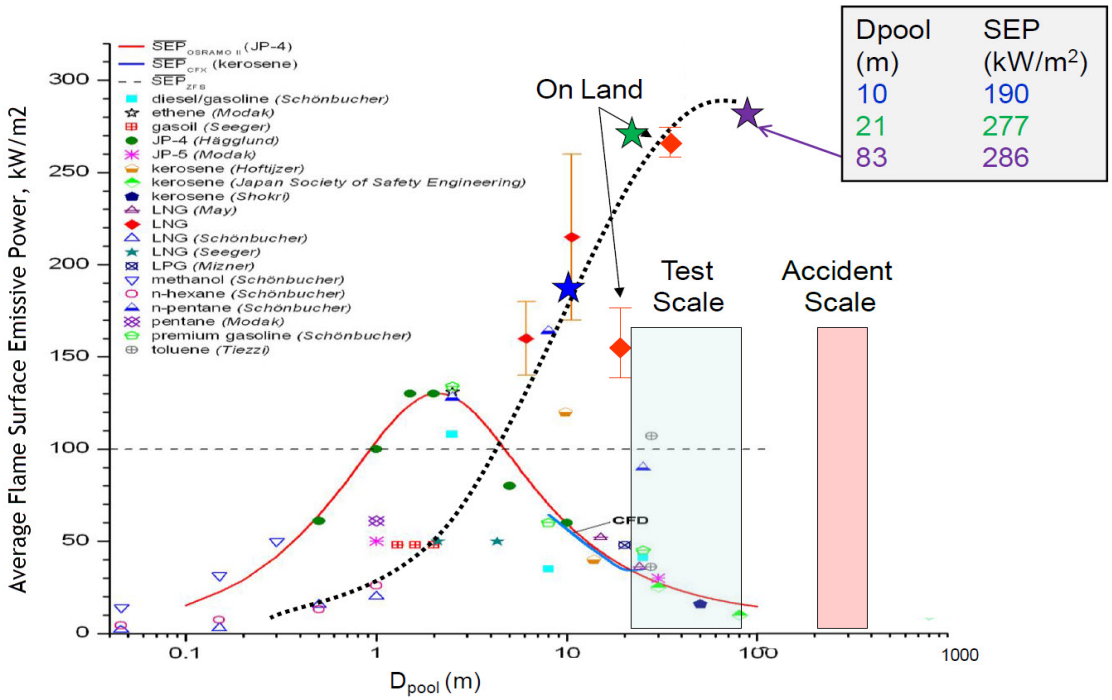

Source: [20, 24]

evaluated at 1,500 K (see Table 9) to yield a value of $\epsilon \simeq 1$:

$$286,000 \quad = \quad \epsilon\sigma T_f^4 \text{ or } \epsilon = \frac{286,000}{5.67 \times 10^{-8} \times 1,500^4} = 0.9963 \tag{16}$$

The consistent values of ϵ and T_f that should be used for large LNG pool fires are $T_f = 1,500$ K and $\epsilon \simeq 1$. These consistent values yield a fraction radiated, χ_r, as outlined by Equation 11:

$$\begin{aligned} \chi_r &= \left(\frac{7,500\ \Delta H_v}{\Delta H_c^2}\right) \epsilon\sigma T_f^4 \\ &= \left(\frac{7,500}{98.04 \times 50.01 \times 10^6}\right) 0.9963 \times 5.67 \times 10^{-8} \times 1,500^4 = 0.437 \text{ or } 43.7\% \end{aligned} \tag{17}$$

7 Burning Rates

As was historically developed by Hottel [2] in 1959 based on data reported by Blinov and Khudiakov [25] in 1957 for pool fires in pans ranging in diameter from 0.4 cm to 3000 cm (30 m), we begin by considering a general energy balance of a burning circular pool in a pan with surface area $A_p = \frac{\pi d^2}{4}$ and liquid depth z_l. The flame provides a steady state heat flux which is transmitted to

the liquid pool surface and used to vaporize the liquid:

$$\frac{\dot{Q}_p}{A_p} = \underbrace{\frac{4k}{d}\left(T_f - T_b\right)}_{\text{conduction}} + \underbrace{U\left(T_f - T_b\right)}_{\text{convection}} + \underbrace{\sigma\chi_{sr}\left(T_f^4 - T_b^4\right)\left(1 - e^{-\kappa d}\right)}_{\text{radiation, } \dot{Q_{sr}}} - \underbrace{\sigma\left(T_b^4 - T_a^4\right)}_{\text{re-radiation}} \tag{18}$$

where $\frac{\dot{Q}_p}{A_p}$ is the net energy flux in $\mathrm{W/m^2}$ that is available to (a) heat the liquid pool material at the pool surface from its initial liquid temperature, T_l, to its boiling point, T_b and to (b) vaporize the liquid to create flammable vapors away from the boiling liquid pool surface. Note that equation 18 does not include heat exchange between the liquid pool and the underlying spill surface. Ground conduction heating rates can be significant for cryogenic liquid spills such as LNG.

The first term in Equation 18 represents heat transfer by conduction from the pan rim at the flame temperature to the liquid in the pan [3]. The pan rim conduction term is only important for fires with very small pool dimensions and decreases linearly with increasing pool diameter. The conduction heat transfer contribution to the overall energy balance for large pools is insignificant for non-cryogenic liquids.

The second term represents convection from the flame to the liquid, the third term represents thermal radiation from the flame, and the last term represents re-radiation heat loss from the liquid surface to the surroundings. In Equation 18, k is the thermal conductivity of liquid in (W/m/K), d is the pool diameter in (m), T_f is the flame temperature above the liquid pool surface in K, T_b is the normal boiling point of the liquid in K, T_a is the ambient temperature in K, $\sigma = 5.67 \times 10^{-8}$ $\mathrm{W/(m^2K^4)}$ is the Stefan-Boltzmann constant, χ_{sr} is the fraction of energy radiated by the flame and is visible to the liquid pool surface, U is an overall convective heat transfer coefficient in $\mathrm{W/m^2/K}$, and κ is Beer's law extinction coefficient of the flame. Blinov and Khudiakov [25] assign a value of 0.25 to χ_{sr} and 5.7 $\mathrm{W/m^2/K}$ to U. These values were based on experimental pool fire data using hydrocarbons.

At small diameters (less than 1 cm) the first term on the right in Equation 18 dominates and causes the burning rate to increase. At large diameters (greater than 100 cm), the first term contribution is small, the second term will be constant, and the third term dominates since κd becomes large and causes the exponential term to go to zero. At intermediate diameters (between 1 and 100 cm), the third term will be low because of the flame thickness and the first term will still be small; thus the burning rate reaches a minimum. This is illustrated in Figure 7. Typical values for burning rates at large diameters are shown in Table 6.

The mass burning rate of the liquid is then estimated from the following equation:

$$\dot{m} = \frac{\dot{Q}_p / A_p}{\Delta H_v + C_{p,l}\left(T_b - T_l\right)} \tag{19}$$

where $\dot{m}$ is the mass burning flux in $\mathrm{kg/m^2/s}$, ΔH_v is the heat of vaporization in $\mathrm{J/kg}$, $C_{p,l}$ is the liquid heat capacity in $\mathrm{J/kg/K}$, and T_l is the liquid pool surface temperature in K. Equation 19 is not directly applicable to mixtures or cryogenic liquids.

For burning mixtures, preferential boiling of light ends causes the mixture bubble point, the mixture heat of vaporization, the mixture flammability limits, and the mixture flame temperature to

[3] The wall cross sectional area is assumed to be equal to the pool area A_p.

Table 6: Experimental large diameter burning velocity and extinction coefficients for different fuels [3]

Fuel	κ (/m)	$\dot{y}$ (m/s)	$\dot{m}$ (kg/m^2/s)
Hexane	1.9	1.22×10^{-4}	
Butane	2.7	1.32×10^{-4}	
Benzene	2.6	1.00×10^{-4}	
Xylene	1.2	0.97×10^{-4}	
Methanol	4.6	0.28×10^{-4}	
UDMH (unsymmetrical dimethyl hydrazone)	2.5	0.63×10^{-4}	
Hydrogen	7.0	2.33×10^{-4}	
LNG	3.0	1.10×10^{-4}	

change as the light ends are vaporized and preferentially depleted from the mixture. In addition, Equation 19 does not apply to burning cryogenic materials where conduction from the underlying spill surface provides additional energy to vaporize the liquid, which can be significant for cryogenic liquids like LNG and LH2.

Transient and detailed material and energy balances (such as those included in the liquid pool models of SuperChems® Expert) can be used for pool fires involving mixtures and cryogenic liquids. The transient energy balances included in SuperChems® Expert have been demonstrated to predict rapid phase transitions for LNG pools [26] where the preferential boiloff of light ends increases the boiling point of the vaporizing mixture, ultimately causing a transition from film boiling to pool boiling accompanied by a large increase in heat transfer rates from the underlying spill surface to the liquid.

For large pool diameters, the third term in Equation 18 dominates and radiative heat transfer to the pool surface drives vaporization of the liquid:

$$\dot{m}_{\max} = \frac{U\left(T_f - T_b\right) + \sigma \chi_{sr}\left(T_f^4 - T_b^4\right)}{\Delta H_v + C_{p,l}\left(T_b - T_l\right)} \tag{20}$$

Several researchers correlated the mass burning rate with the ratio of heat of combustion to heat of vaporization. The form is consistent with Equation 20. Figure 8 shows the dependency of measured burning rate data (at large diameters) on this ratio for several materials.

In Figure 8 the burning velocity of a liquid pool is the rate at which the pool level decreases with time. The mass burning rate is a related term, being a product of the burning velocity and the fuel liquid density. Careful examination of Figure 8 shows that materials like LNG and LH2 would require quantification of the transient and spill surface geometry and roughness dependent additional heat gained by ground conduction.

Extensive burn rate measurements [27] have shown a definite relationship between the burning velocity and thermochemical fuel properties, such as the ratio of the net heat of combustion and

Figure 7: The dependence of burning rate on pool diameter [2, 3]

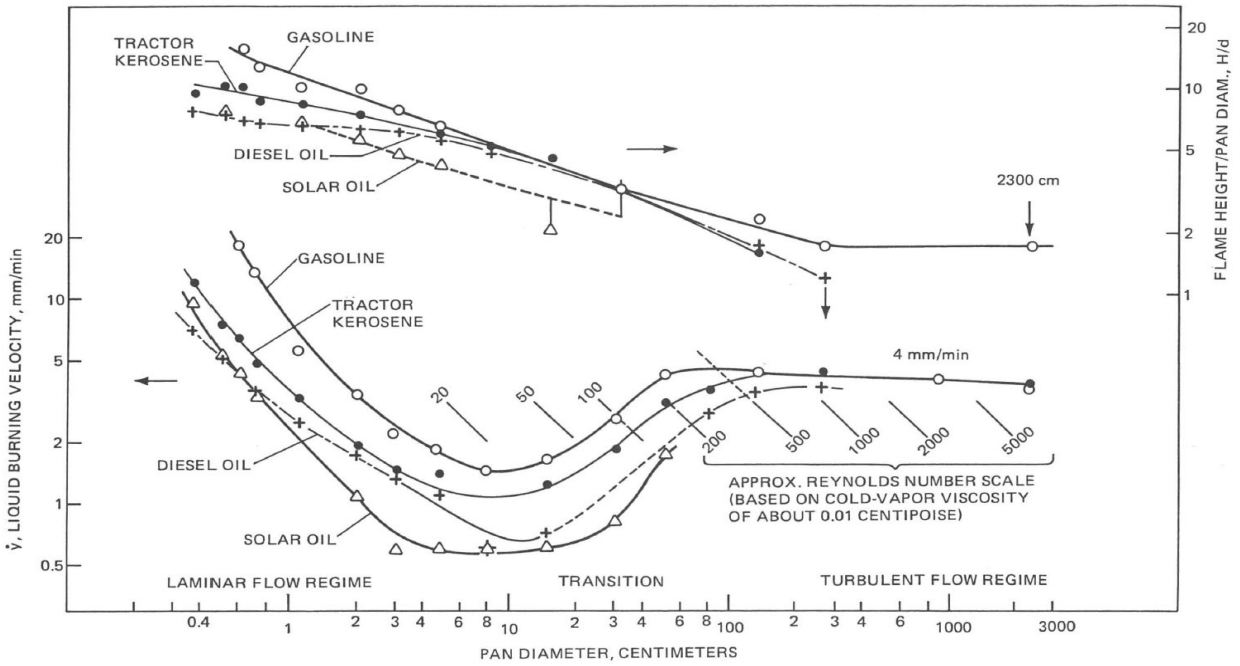

vaporization (see Equations 19 and 20). The relationship used to estimate the burning rate is:

$$\dot{m}_{\max} = 0.001 \frac{\Delta H_c}{\Delta H_v} \tag{21}$$

$$\dot{y}_{nbp} = \frac{\dot{m}_{\max}}{\rho_{l,nbp}} \quad \text{or} \quad \dot{y}_{\rho_l} = \frac{\dot{m}_{\max}}{\rho_l} \tag{22}$$

where, $\dot{y}$ in the liquid burning velocity or regression rate in $\mathrm{m/s}$, ΔH_c is standard heat of combustion in $\mathrm{kJ/kg}$, ΔH_v is the heat of vaporization at the boiling point in $\mathrm{kJ/kg}$, $\rho_{l,nbp}$ is the pool surface liquid density at the normal boiling point in $\mathrm{kg/m^3}$, and ρ_l is the liquid density at the pool bulk liquid temperature $\mathrm{kg/m^3}$.

Where measured values of burning rates exist ($\dot{m}$ or $\dot{y}$), we can use Equation 18 to calculate the fraction of heat radiated and convected back to the liquid pool surface:

$$\chi_{sr} = \frac{\dot{m}\left[\Delta H_v + C_{p,l}\left(T_b - T_l\right)\right] - \frac{4k}{d}\left(T_f - T_b\right) - U\left(T_f - T_b\right) + \sigma\left(T_b^4 - T_a^4\right)}{\sigma\left(T_f^4 - T_b^4\right)\left(1 - e^{-\kappa d}\right)} \tag{23}$$

In the absence of measured burning rate data one can always use Equation 21 (also see Figure 8) to estimate the burning rate and then use Equation 23 to calculate χ_{sr}.

A maximum burning rate, $\dot{m}_{\max}$ is reached at large pool diameters as shown by Equation 18. Some authors have suggested a simple equation to correlate mass burning rate with pool diameter [5]:

$$\dot{m} = \dot{m}_{\max}\left[1 - \exp\left(-\beta\kappa d\right)\right] \tag{24}$$

where $\beta\kappa$ is the product of a mean beam length corrector and the flame extinction coefficient in $\mathrm{m^{-1}}$. Table 7 provides a summary of measured burning rate data for a variety of fuels for pool

Figure 8: The dependence of burning rate* on the ratio of heat of combustion to heat of vaporization, $\frac{\Delta H_c}{\Delta H_v}$

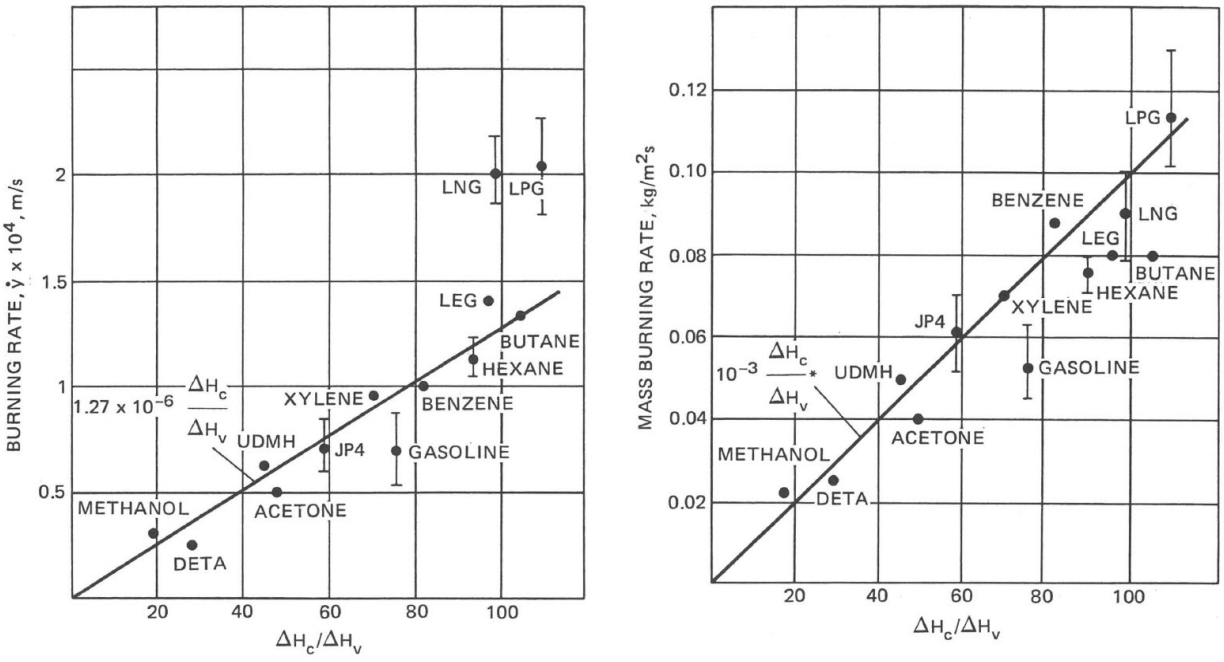

Source: [3]; *: Pool fires on land; UDMH is unsymmetrical dimethyl hydrazone; DETA is diethylene triamine; LEG is liquefied ethylene gas.

diameters ranging from 0.6 to 35 meters, wind speeds up to 9.6 m/s, and relative humidity data ranging from 23 to 87 %.

8 Flame Emissive Power

The emissive power of a large turbulent fire is a function of the blackbody emissive power and the flame emissivity. The blackbody emissive power, in turn, can be computed using Planck's law of radiation, if the mean radiation flame temperature, T_f, is known. For incident flux calculations, however, it is more important to estimate the effective emissive power of the flame, which accounts for shielding by surrounding layers of smoke for liquid hydrocarbon fires.

Large scale pool fire data collected during the last decade indicate that the flame zone above the liquid surface is sustained at the limit temperature corresponding to the upper flammability limit (see Table 8). Equation 20 can be used to check the consistency of reported upper flammability limits and burning rates.

Figure 9 summarizes numerous thermochemical equilibrium calculations for several compounds. The X axis represents the mole fraction of fuel in air. The flame adiabatic temperatures were calculated using a starting temperature of 298.15 K at 1 bara.

Table 7: Measured burning rate and extinction coefficients for different fuels [5]

Fuel	$\dot{m}_{\max}$, $\mathrm{kg/m^2/s}$	$\kappa\beta$, $\mathrm{m^{-1}}$	E_p, $\mathrm{kW/m^2}$	κ, $\mathrm{m^{-1}}$
Acetone	0.038	2.238	130	
Benzene	0.085	2.700	130	
Butane	0.110	0.852	225	0.937
Crude oil	0.051	1.301	130	
Diesel	0.054	1.301	130	
Ethane	0.141	0.136	250	0.149
Ethanol	0.020		130	
Fuel oil	0.034	1.670	130	
Gasoline	0.067	1.480	130	
Heptane	0.081	1.394	200	
Hexane	0.075	1.394	200	
Hydrogen	0.161	6.741	70	7.415
JP4	0.056	1.962	130	
JL5/kerosene	0.063	1.296	130	
Ethylene	0.140		265	
LNG/methane	0.141	0.136	265	0.149
LNG/methane (water)	0.282		265	
LPG/propane	0.118	0.500	250	0.550
LPG/propane (water)	0.256		250	
Methanol	0.020		70	
Naptha/pentane	0.095		200	
Octane	0.081	1.394	200	
Toluene	0.066	3.370	130	
Xylene	0.090	1.400	130	

Based on observed values of emissive powers reported in the literature and other available data (Haggland et al. [28] and Alger et al. [29]), the effective emissive power (for hydrocarbons only) was correlated to the normal boiling point by the expression:

$$E_p = \max\left(117 - 0.313\ T_{\text{NBP}}, 20\right) = \frac{\epsilon\sigma T_f^4}{1000} \tag{25}$$

where E_p is the hydrocarbon effective emissive power in $\mathrm{kW/m^2}$ and T_{NBP} is the hydrocarbon normal boiling point in $^\circ\mathrm{F}$.

As illustrated in Table 8, the flame zone above the liquid surface of a pool fire is sustained at the limit temperature corresponding to the upper flammability limit, $\simeq 1,500$ K for hydrocarbons. Using Equation 25, we can calculate an implied effective flame emissivity of hydrocarbon pool fires, ϵ. This is shown in Table 9. Note the upper flammability limit also depends on temperature [4].

Mudan and Croce [3] proposed a more general equation for heavy hydrocarbons to account for

[4] $UFL \simeq UFL_{298.15K} + \frac{0.75}{\Delta H_c}(T - 298.15)$, where UFL is in volume %, T is in K, and ΔH_c is in kcal/gmol.

Table 8: Measured flame surface temperature of pool fires vs. calculated flame temperature values at the upper flammability limit (UFL)

Fuel	Measured, K	Predicted @298.15 K	Predicted @NBP	UFL @NBP, Vol %
Acetone				
Methanol				
Glycerol				
Triolein				
Methyl Oleate				
Ethanol	1,560	1,552		19
Benzene	1,460	1,430		7.4
Petrol	1,520			
Kerosine	1,480			
Mixed Solvent	1,500			

NBP: Calculated at a starting temperature of fuel normal boiling point.

smoke and soot production by the flame:

$$E_p = xE_f + (1-x)E_s \tag{26}$$

where x is the luminous fraction of the flame surface and E_s is the smoke/soot emissive power $\simeq 20\ \mathrm{kW/m^2}$.

9 Incident Flux Calculation

The incident flux at any given location or surface is given by the equation:

$$I = \tau F_m E_p - \epsilon_s \frac{\sigma T_s^4}{1000} = \tau F_m \chi_r \frac{\sigma T_f^4}{1000} - \epsilon_s \frac{\sigma T_s^4}{1000} \tag{27}$$

where I is the surface incident flux in $\mathrm{kW/m^2}$, E_p is the flame emissive power in $\mathrm{kW/m^2}$, ϵ_s is the surface emissivity, T_s is the surface or surroundings temperature in K, τ is the atmospheric transmissivity, and F_m is maximum geometric view factor between the flame and receiving surface. Detailed methods for calculating atmospheric transmissivity and geometric view factors for cylindrical and rectangular flames are included in the fire models of SuperChems® Expert . They are also accessible by user defined scripts using TEAL.

10 Pool Spreading

The spectrum of hydrocarbon liquid spill scenarios is wide. Spills can be classified based on the rate of release and duration:

Figure 9: Calculated adiabatic flame temperatures for selected fuels as a function of fuel mole fraction - balance is air

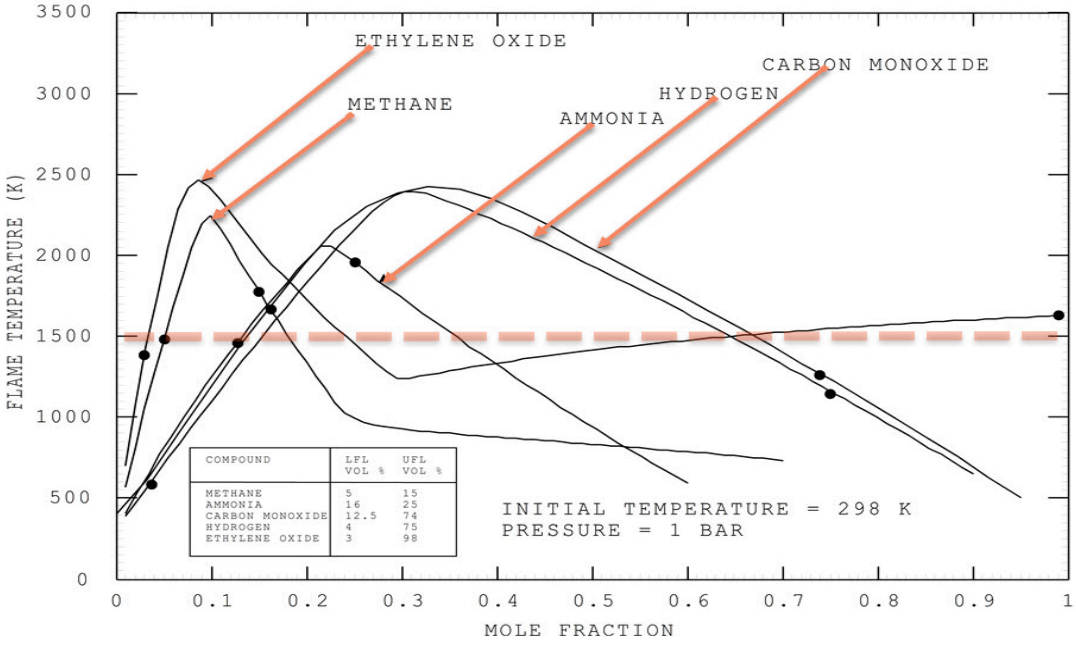

Source: SuperChems® Expert

- Continuous spills - in which the spill continues at a specified finite rate for a long duration.
- Instantaneous spills - in which all of the spill occurs over a *very* short time.
- Finite duration spills - where a given volume of liquid is spilled over a given duration of time. Both the release rate and the release duration are finite.

SuperChems® Expert solves the transient shallow water equations [23] to determine the extent of pool spreading on land or water. The transient solution includes detailed representations of heat and mass transfer mechanisms including solar radiation, conduction from the underlying spill surface, and heating from the flame for a burning pool for single components and mixtures. The preferential boil off of light ends includes the vapor/liquid equilibrium of non-ideal mixtures and mixtures with azeotropes.

A burning pool will reach an equilibrium pool diameter at the point where the liquid feed rate to the pool equals the burning rate. The flame height and pool fire duration will depend on when the pool is ignited. An immediate ignition causes the pool to spread to an equilibrium diameter where the feed rate equals the burning rate. However, a delayed ignition that occurs after the pool spreads to an equilibrium diameter where the feed rate equals the evaporation or vaporization rate, causes the flame height to be higher and the fire duration to shorter as the pool depth will be smaller.

We illustrate pool burning and spreading for a release of cyclohexane on a concrete surface. We vary the spill rate from 0.1 to 100 kg/s (794 lb/hr to 794,000 lb/hr) and ignite the pool 1 minute after the release starts. We use a wind speed of 2 m/s and a relative humidity is 70 % at a visual range of 6,600 feet (2,011 m). The SuperChems® Expert simulation results are shown in Figures 10 and

Table 9: Calculated emissive power of normal hydrocarbons from Equation 25 for large pool fire diameters (> 1 meter) and a flame temperature of 1,500 K

Fuel	Carbon Number	Normal Boiling Point, °F	E_p, $\mathrm{kW/m^2}$	ϵ
Blackbody			288	1.000
Methane	C_1	-258.68	198	0.687
Ethane	C_2	-127.48	157	0.545
Propane	C_3	-43.67	131	0.454
Butane	C_4	31.10	107	0.371
Pentane	C_5	96.92	87	0.302
Hexane	C_6	155.71	68	0.236
Heptane	C_7	209.17	52	0.180
Octane	C_8	258.22	36	0.125
Nonane	C_9	303.48	22	0.076
Decane	C_{10}	345.48	20	0.069
Soot and Heavier Hydrocarbons	$> C_{10}$	> 345.48	20	0.069

11. We note from Figure 10 that a flame height of 30 ft (9.2 m) is reached with a small release rate of less than 1,000 lb/hr (0.126 kg/s). Additional simulation results are shown in Table 10.

11 Flame Height

A burning pool flame height value is necessary for thermal radiation and safe separation distance evaluations. Thomas [30] has developed a correlation for the mean visible flame height of turbulent diffusion flames in the presence of wind:

$$\frac{L_f}{D_p} = \frac{55}{u_*^{0.21}} \left(\frac{\dot{m}}{\rho_a \sqrt{g\ D_p}} \right)^{0.67} \tag{28}$$

where, L_f is the mean visible flame height in m, D_p is the pool diameter in m, $\dot{m}$ is the mass burning rate per unit pool area in $\mathrm{kg/m^2 \cdot s}$, and ρ_a is the ambient air density in $\mathrm{kg/m^3}$, and u_* is the non-dimensional wind velocity given by:

$$u_* = \frac{u_w}{\left(\frac{g \dot{m} D}{\rho_v} \right)^{1/3}} \tag{29}$$

g is the acceleration due to gravity in $\mathrm{m/s^2}$ and ρ_v is the vapor density of fuel in $\mathrm{kg/m^3}$ at ambient conditions. A simpler correlation for flame height is proposed by Bubbico [31] which only depends on pool diameter:

$$\frac{L_f}{D_p} = 1.73 + \frac{0.33}{D_p^{1.43}} \tag{30}$$

where D_p is the burning pool diameter in m.

Figure 10: Calculated maximum pool diameter and flame height for a cyclohexane spill using SuperChems® Expert

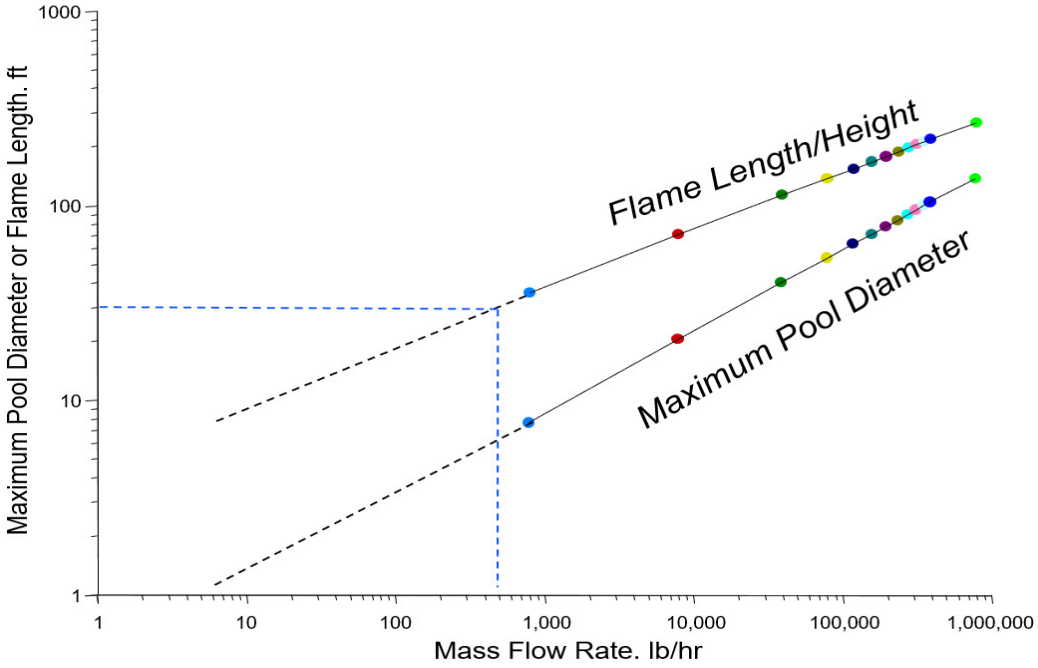

Source: SuperChems® Expert

12 Flame Tilt

Wind can cause the flame of a burning pool to bend or tilt. The upper portions of a tilted or inclined flame will be closer to an observer location downwind of the burning pool (higher thermal radiation incident flux) and further from an observer located upstream of the burning pool (lower thermal radiation incident flux). The angle of tilt (θ) of the flame from the vertical is given by (American Gas Association [32]):

$$\cos\theta = \begin{cases} 1 & \text{for } u_* \leq 1 \\ u_*^{-0.5} & \text{for } u_* > 1 \end{cases} \tag{31}$$

where, u_* is given by Equation 29.

13 Flame Drag

Under high wind conditions, a burning pool flame can tilt and drag in into the downwind direction. Flame drag is defined as the distance by which the base of the flame is extended downwind, while the upwind edge of the flame and the flame width remain unchanged. When flame drag occurs, the flame will be closer to an observer located downwind from the flame, i.e., higher thermal radiation will be received by that observer due to flame tilt and drag. Flame drag is a strong function of wind

Figure 11: Calculated time history of pool diameter for a cyclohexane spill using SuperChems® Expert

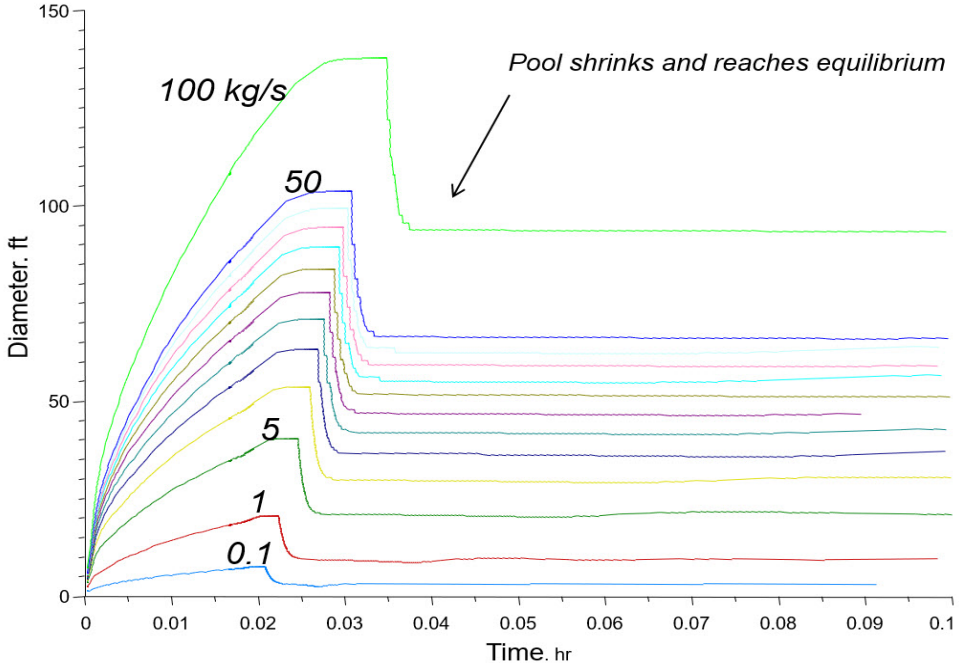

Source: SuperChems® Expert

speed. The correlation used to predict flame drag is given by (Mudan [33]):

$$D' = 1.25 D_p \mathrm{Fr}_{10}^{0.069} \left(\frac{\rho_v}{\rho_a} \right)^{0.48} \tag{32}$$

where the Froude number Fr_{10} is calculated based upon the wind speed at a height of 10 m:

$$\mathrm{Fr}_{10} = \frac{u_{w10}^2}{g\ D_p} \tag{33}$$

where u_{w10} is the 10 m wind speed in $\mathrm{m/s}$.

14 Conclusions

The API-521 [4, 6] proposed default average and peak values of ϵ and T_f for use with Annex A equation A.1 are most suitable for hydrocarbons (see Table 2). They are not suitable for large pool fires of hydrogen (LH2), LNG, and low carbon number alcohols such a methanol and ethanol. The recommended peak values for LNG are $\epsilon \simeq 1$, $T_f \simeq 1,500$ K. The recommended values for ethanol are $\epsilon \simeq 0.18$, $T_f \simeq 1,273$ K.

Table 10: Additional simulation results for cyclohexane liquid release and pool fire

Flow Rate. Kg/s	Maximum Pool Fire Diameter. m	Maximum Flame Height. m	Flame Tilt. Degrees	Flame Drag. m	Flame Emissive Power. kW/m^2	Distance to 5 kW/m^2 from Pool Edge. m	Distance to 12.5 kW/m^2 from Pool Edge. m
1	6.3	21.6	33	1.5	62	21	11
5	12.3	34.4	21	2.3	62	31	15
10	16.3	41.8	12	2.7	62	35	16
15	19.2	50.0	0	2.9	62	35	15
20	21.6	51.0	0	3.0	62	38	16
25	23.7	54.3	0	3.2	62	41	17
30	25.5	57.2	0	3.3	62	43	18
35	27.3	59.8	0	3.4	62	45	19
40	28.8	62.1	0	3.4	62	47	20
45	30.2	64.3	0	3.5	62	49	21
50	31.2	66.3	0	3.5	62	51	22
100	42.0	81.0	0	3.8	62	63	26

Source: SuperChems® Expert

15 Recommended Additional Reading

Please refer to additional ioMosaic® publications in the fire modeling series for more details on understanding thermal radiation modeling and atmospheric transmissivity, the calculation of geometric view factors for solid flame geometries, the calculation of flame emissive power and fraction radiated for pool fires and flame jets/flares, the calculation of short duration exposure to thermal radiation from fireballs and vapor cloud fires, the dynamics of pressure relief under fire exposure, and estimated time to failure or yield for vessels exposed to internal heating by runaway reaction(s) and/or external heating by fire. These technical publications can be made available upon request.

16 References

[1] A. Hammins, T. Kashiwagi, and R. Burch. Characteristics of pool fire burning. In *Fire Resistance of Industrial Fluids*. ASTM, June 1995.

[2] H. Hottel. Review: Certain laws governing diffusive burning of liquids by Blinov and Khudiakov (1957). *Fire Research Abstracts and Reviews*, 1:41–44, 1959.

[3] K. S. Mudan and P. A. Croce. Fire hazard calculations for large open hydrocarbon fires. In *The SFPE Handbook of Fire Protection Engineering, Section 2, Chapter 4*. NFPA, 1988.

[4] API. *API Standard 521 - Pressure Relieving and Depressuring Systems*. American Petroleum Institute, 7th edition, 2020.

[5] P. J. Rew, W. G. Hulbert, and D. M. Davies. Modelling of thermal radiation from external hydrocarbon pool fires. *Trans IChemE*, 75(B):81–89, 1997.

[6] API. *API Standard 521 - Pressure Relieving and Depressuring Systems*. American Petroleum Institute, 6th edition, 2013.

[7] G. A. Melhem. RAGAGEP considerations for overtemperature protection in relief systems. *ioMosaic Corporation Publication*, December 2021.

[8] G. A. Melhem. Are pool fires only 25 ft high? In *DIERS Users Group Meeting*. AIChE, Spring 2008.

[9] NFPA 30. Flammable and combustible liquids code, 2015.

[10] G. A. Melhem. Proper calculations of pipe and vessel wall temperatures during relief and/or depressurization. In *78th API Fall Refining and Equipment Standards Meeting*, pages 221–226, November 2013.

[11] B. Droste and W. Schoen. Full-scale fire tests with unprotected and thermal insulated LPG storage tanks. *Journal of Hazardous Materials*, 20:41–53, 1988.

[12] W. Schoen and B. Droste. Investigation of water spraying systems for LPG storage tanks by full-scale fire tests. *Journal of Hazardous Materials*, 20:73–82, 1988.

[13] G. A. Melhem, P. A. Croce, and H. Abraham. Data summary and analysis of NFPA's BLEVE tests. *Process Safety Progress*, 12(2):76–82, 1993.

[14] K. McGrattan, H. Baum, and A. Hamins. Thermal radiation from large pool fires. Technical Report NISTIR 6546, NIST, November 2000.

[15] P. Hooker, D. Willoughby, J. Hall, and M. Royle. Experimental releases of liquid hydrogen. In *Hazards XXIII Symposium Series No. 158*, pages 496–504. IChemE, 2012.

[16] C. Bernardy, A. K. Habib, M. Kluge, B. Schalau, and H. Kant. Large-scale investigations of thermal radiation of hydrogen jet flames. *Journal of Loss Prevention in the Process Industries*, 94:1–6, 2025.

[17] Sun Chan Kim, Ki Young Lee, and Anthony Hamins. Energy balance in medium-scale methanol, ethanol, and acetone pool fires. *Fire Safety Journal*, 107:44–53, July 2019.

[18] National Research Council of Canada. Fire tests of distillate spirit storage tanks. client report cr-5727.1, 1989.

[19] D. Nedelka, J. Moorhouse, and R. Tucker. The Montoir 35-m diameter LNG pool fire experiments. In *LNG 9*. International Conference on Liquefied Natural Gas, Nice, France, 1989.

[20] T. Blanchat. The Phoenix series large scale LNG pool fire experiments. Technical Report SAND2010-8676, Sandia National Laboratories, December 2011.

[21] A. Luketa. Recommendations on the prediction of thermal hazard distance from large liquified natural gas pool fires on water for solid flame models. Technical Report SAND2011-9415, Sandia National Laboratories, December 2011.

[22] G. A. Melhem. Reducing uncertainty in LNG fire exposure modeling. In *LNG Topical Conference*. AIChE/CSChE, August 2009.

[23] S. Saraf and G. A. Melhem. Modeling LNG pool spreading and vaporization. In *5th Topical Conference on Natural Gas Utilization Meeting, Atlanta, Georgia*. American Institute of Chemical Engineers AIChE, 2005.

[24] Hyunjoo Chun, Klaus-Dieter Wehrstedt, Iris Vela, and Axel Schönbucher. Thermal radiation of di-tert-butyl peroxide pool fires: Experimental investigation and cfd simulation. *Journal of Hazardous Materials*, 167(1-3):105–113, 2009.

[25] V. Blinov and G. Khudiakov. Diffusion burning of liquids. Translation NTIS AD-296762, Academy of Sciences, 1961.

[26] G. A. Melhem, H. Ozog, and S. Saraf. Understand LNG rapid phase transitions. *Hydrocarbon Processing*, 85:53–59, 2006.

[27] D. S. Burgess, A. Strasser, and J. Grumer. Diffusive burning of liquid fuel in open trays. *The Fire Research Abs. & Review*, 3:177, 1961.

[28] B. Haggland and L. Person. The heat radiation from petroleum fires. Foa rapport, Forsvarets Forskningsanstalt, Stockholm, 1976.

[29] R. S. Alger, R. C. Corlett, A. S. Gordon, and F. A. Williams. Some aspects of turbulent pool fires. *Journal of Fire Technology*, 15(2):142–156, 1979.

[30] P. H. Thomas. The size of flames from natural fires. *9th International Combustion Symp.*, pages 844–859, 1963.

[31] R. Bubbico, G. Dusserre, and B. Mazzarotta. Calculation of the flame size from burning liquid pools. *Chemical Engineering Transactions*, 53:67–72, January 2016.

[32] American Gas Association. LNG safety research program. Technical report, American Gas Association, 1974. Report IS 3-1.

[33] K. S. Mudan. Thermal radiation hazards from hydrocarbon pool fires. *Prog. Energy Comb. Sci.*, 10:59–80, 1984.

....

Index

About the Authors

Dr. Melhem is an internationally known pressure relief and flare systems, chemical reaction systems, process safety, and risk analysis expert. In this regard he has provided consulting, design services, expert testimony, incident investigation, and incident reconstruction for a large number of clients. Since 1988, he has conducted and participated in numerous studies focused on the risks associated with process industries fixed facilities, facility siting, business interruption, and transportation.

Prior to founding ioMosaic® Corporation, Dr. Melhem was president of Pyxsys Corporation; a technology subsidiary of Arthur D. Little Inc. Prior to Pyxsys and during his twelve years tenure at Arthur D. Little, Dr. Melhem was a vice president of Arthur D. Little and managing director of its Global Safety and Risk Management Practice and Process Safety and Reaction Engineering Laboratories.

Dr. Melhem holds a Ph.D. and an M.S. in Chemical Engineering, as well as a B.S. in Chemical Engineering with a minor in Industrial Engineering, all from Northeastern University. In addition, he has completed executive training in the areas of Finance and Strategic Sales Management at the Harvard Business School. Dr. Melhem is a Fellow of the American Institute of Chemical Engineers (AIChE) and Vice Chair of the AIChE Design Institute for Emergency Relief Systems (DiERS).

Contact Information

Georges. A. Melhem, Ph.D., FAIChE
E-mail. melhem@iomosaic.com

ioMosaic Corporation
93 Stiles Road
Salem, New Hampshire 03079
Tel. 603.893.7009, x 1001
Fax. 603.251.8384
web. www.iomosaic.com

How can we help?

Please visit www.iomosaic.com and www.iokinetic.com to preview numerous publications on process safety management, chemical reactivity and dust hazards characterization, safety moments, video papers, software solutions, and online training.

In addition to our deep experience in process safety management (PSM), chemical reaction systems, and the conduct of large-scale site wide relief systems evaluations by both static and dynamic methods, we understand the many non-technical and subtle aspects of regulatory compliance and legal requirements. When you work with ioMosaic® you have a trusted ISO certified partner that you can rely on for assistance and support with the lifecycle costs of relief systems to achieve optimal risk reduction and PSM compliance that you can evergreen. We invite you to connect the dots with ioMosaic®.

We also offer laboratory testing services through ioKinetic® for the characterization of chemical reactivity and dust/flammability hazards. ioKinetic® is an ISO accredited, ultramodern testing facility that can assist in minimizing operational risks. Our experienced professionals will help you define what you need, conduct the testing, interpret the data, and conduct detailed analysis. All with the goal of helping you identify your hazards, define and control your risk.

ioMosaic®
Minimizing risk. Maximizing potential.®

About ioMosaic Corporation

Our mission is to help you protect your people, plant, stakeholder value, and our planet.

Through innovation and dedication to continual improvement, ioMosaic has become a leading provider of integrated process safety and risk management solutions. ioMosaic has expertise in a wide variety of disciplines, including pressure relief systems design, process safety management, expert litigation support, laboratory services, training, and software development.

As a certified ISO 9001:2015 Quality Management System (QMS) company, ioMosaic offers integrated process safety and risk management services to help you manage and reduce episodic risk. Because when safety, efficiency, and compliance are improved, you can sleep better at night. Our extensive expertise allows us the flexibility, resources, and capabilities to determine what you need to reduce and manage episodic risk, maintain compliance, and prevent injuries and catastrophic incidents.

Consulting Services

- Asset Integrity
- Auditing
- Due Diligence
- Facility Siting
- Fault Tree/SIL Analysis
- Fire & Explosion Dynamics
- Incident Investigation, Litigation Support, and Expert Testimony
- Hydrogen Safety
- LNG Safety
- LPG Safety
- Pipeline Safety
- Process Hazard Analysis
- Process Engineering Design and Support
- Process Safety Management
- Relief and Flare Systems Design and Evaluation
- Risk Management Program Development
- Quantitative Risk Assessment
- Software Solutions
- Structural Dynamics
- Sustainability Reporting Support
- Technology Transfer Package Development
- Process Safety Training

Laboratory Testing Services (ISO Accredited)

- Battery Safety Testing
- Chemical Reactivity Testing
- Combustible Dust Hazard Analysis and Testing
- Flammability Testing
- Physical Properties Testing
- Process Safety Services
- Specialized Testing

US Offices

Salem, New Hampshire
Houston, Texas
Minneapolis, Minnesota
Berkeley, California

International Offices

Al Seef, Kingdom of Bahrain
Bath, United Kingdom

Software Solutions

Process Safety Office®: A suite of integrated tools for process safety professionals and risk analysts.

Process Safety Enterprise®: Process Safety Management compliance made easy with enterprise workflows, dynamic forms, document management, key performance indicators and metrics, and more.

Process Safety Learning®: Build your process safety competencies incrementally using learning modules.

Process Safety tv®: The worldś first video streaming platform dedicated to process safety.

Contact us

www.ioMosaic.com
sales@ioMosaic.com
1.844.ioMosaic